6ICEGE
6th International Conference on Earthquake Geotechnical Engineering
1-4 November 2015
Christchurch, New Zealand

Insights into the Seismically-Induced Rock-slope Failures in the Canterbury Region Using the Discrete Element Method

L. Arnold[1], J. Wartman[2], C. Massey[3], M. MacLaughlin[4], D. Keefer[5]

ABSTRACT

During the Canterbury Earthquake sequence in New Zealand, the greater Christchurch area experienced several rock-slope failures which resulted in 5 casualties and significant loss of inhabitable property. As a part of the U.S. National Science Foundation-supported Network for Earthquake Engineering Simulation (NEES) project *Seismically-induced rock-slope failures: mechanisms and prediction* (NEESROCK), two sites in the Port Hills area were selected for dynamic modeling using the particulate discrete element code PFC. The discrete element model is able to simulate intact rock strength, explicitly defined discontinuities, the development of damage in the rock mass, and the transmission and reflection of dynamic waves. Results simulations show strong agreement with the observed cliff collapse behavior at the sites as measured in the field, however, the simulations do not capture the cliff top surface displacement.

Introduction

During the Canterbury Earthquake sequence, in New Zealand, rock-slope failures resulted in loss of life and significant loss of inhabitable property. Damage in rock-slopes during these events, was characterized by two key features: 1) *Cliff collapse*, where a relatively shallow failure of intact or partially intact rock along the cliff face fails, and 2) *Cliff top displacement*, made evident by cracking of the ground behind the slope crest indicating a large mass movement (Massey et al. 2014(a), Massey et al, 2012).

Traditional limit equilibrium and/or Newmark sliding block methods are often sufficient to model a deep-seated (i.e., large mass) failure and predict or replicate its deformation due to strong ground motion. The small mass *cliff collapse* mechanism, however, which in the Canterbury earthquake sequence accounted for the most violent and devastating rock-slope responses, are neither predicted nor explained by traditional methods. When traditional or simplified methods are inadequate to explain complex phenomena, advanced numerical methods may be required to capture the desired behavior.

The discrete element method (DEM), and particularly a subset of DEM called the bonded particle method (BPM) has become widely used for modelling complex rock mechanics problems. BPM, first introduced by Potyondy and Cundall in 2004, has been shown to accurately reproduce several complex rock behaviors. The DEM code PFC was used to develop the models in this paper.

[1]Lorne Arnold, Civil Engineering, University of Washington, Seattle, United States, lorne87@uw.edu
[2]Joseph Wartman, Civil Engineering, University of Washington, Seattle, United States, wartman@uw.edu
[3]Chris Massey, GNS Science, Wellington, New Zealand, c.massey@gns.cri.nz
[4]Mary MacLaughlin, Montana Tech, Butte, United States, mmaclaughlin@mtech.edu
[5]David Keefer, University of Maine, United States, davidkkeefer@gmail.com

New Zealand Sites

Cross-sections from two sites, Redcliffs and Richmond Hill, were selected for modeling. These sites were selected because both *cliff collapse* (as shown in Figure 1) and *cliff top displacement* were observed following strong ground motion, the sites have relatively two-dimensional cliff face sections, and they have been well characterized by field and laboratory testing.

Richmond Hill

The Richmond Hill site is located on a volcanic spur with a very steep cliff face on one side and a fairly gentle (~30 degrees) slope on the other. The cliff itself is about 50 meters high and 540 meters long with a slope angle between 50 degrees and 90 degrees. A wide section of the cliff face can be characterized by 3 main geologic units. From top to bottom they are: 1) Blocky columnar jointed basalt lava, 2) Trachy lava breccia, 3) Trachy basalt lava.

Redcliffs

The Redcliffs site is a 60 meter high cliff with a slope angle between 50 and 80 degrees. A section of the cliff face can be characterized by 4 main geologic units. From top to bottom they are: 1) Basalt lava breccia, 2) Columnar jointed basalt lava and breccia, 3) Epiclastics, and 4) a second layer of basalt lava breccia.

Figure 1. Cliff collapse at the Richmond Hill (left) and Redcliffs (right) sites after the February 22, 2011 earthquake. [photo credit: GNS Science]

A more complete assessment of the two sites can be found in the GNS Science reports on risk assessment for the two sites (Massey et al., 2014(b) and Massey et al. 2014(c)).

Model Details

Three rock-slope geometries were built and evaluated in PFC: 1) a generic rock-slope model made up of a single material without any pre-existing fractures, and site specific models for 2) the Richmond Hill and 3) the Redcliffs sites. The generic model was not tested to failure, instead it was subjected to a single shear wavelet pulse for the purpose of observing the stresses in the slope as the pulse passed through.

Engineering properties have been assigned to the geologic units at the sites based on laboratory and field tests from drillhole core samples and fallen boulders. Two estimates of engineering properties have been adopted: 1) an 'average' estimate, and 2) a reasonable 'lower-bound' estimate for strength and modulus. In general, the 'average' estimates were taken from the testing of boreholes and the 'lower' estimates were taken from fallen boulders (Massey et al., 2014(c)). Both average and lower estimates for strength were incorporated into the bonded-particle models. The majority of the slope was given the average engineering properties and the face of the slope was given the lower estimate properties in a discrete 'weathered' zone. From the face of the slope to the edge of the weathered zone (20 meters in width), the engineering properties were increased so that 20 meters into the slope face, the engineering properties matched the average values. Table 1 shows the average and lower estimates for the engineering properties for each layer in the site models.

Table 1. Average and lower estimates for engineering properties of intact materials at the Richmond Hill (RH) and Redcliffs (RC) sites. UCS is unconfined compressive strength, σ_t is tensile strength, E is the elastic modulus, V_s is the shear wave velocity, and ρ is density.

	Layer	UCS [MPa]	σ_t [MPa]	E [GPa]	V_s [m/s]	ρ [kg/m^3]
Average	Columnar Basalt Lava (RH)	55.0	5.7	12.0	1500	2800
	Trachy Lava Breccia (RH)	5.0	0.7	3.8	1500	2200
	Trachyte Basalt Lava (RH)	150.0	10.5	13.0	2300	2600
	Upper Breccia (RC)	1.7	0.3	0.2	800	1800
	Columnar Basalt Lava (RC)	200.0	12.0	8.5	1700	2800
	Epiclastics (RC)	4.7	0.5	0.3	1000	1900
	Lower Breccia (RC)	2.7	0.4	0.5	700	1900
Lower	Columnar Basalt Lava (RH)	20.0	5.7	10.0	1400	2800
	Trachy Lava Breccia (RH)	3.0	0.7	1.0	800	2200
	Trachyte Basalt Lava (RH)	101.0	10.5	10.0	2000	2600
	Upper Breccia (RC)	1.3	0.2	0.1	600	1800
	Columnar Basalt Lava (RC)	150.0	10.0	3.4	1100	2800
	Epiclastics (RC)	3.7	0.4	0.3	1000	1900
	Lower Breccia (RC)	1.8	0.3	0.4	600	1900

Other than the columnar basalt layers, the natural fractures in the rock-slopes were very irregular. An approximation of fracture frequency and extent based on drilled borings was made and applied to the BPM using the smooth-joint contact method developed by Mas Ivars et al. (2011). The columnar basalt layers were given a 3 meter joint spacing and 20 meter joint lengths with a vertical orientation and 5 meter rock bridge lengths. All other layers where given a 20 meter joint spacing and 10 to 20 meter joint lengths with random orientation. The 3 meter spacing in the columnar basalt layers is wider than what was observed in the field. However, 3 meters was determined to be the minimum allowable spacing for the given size of particles used in the model.

For the two site-specific model geometries, four unique models of each site were generated by

varying the random packing of particles in the model. By evaluating multiple models with unique particle arrangements but which are otherwise identical, the sensitivity of the model result to the particle structure can be evaluated.

Typical engineering properties cannot be applied directly to the bonded-particle model. An extensive calibration process is needed, which identifies the micro-properties required to achieve the desired macro-properties. BPM inputs include particle size, particle friction, particle and bond stiffnesses in the normal and shear directions, and bond normal and shear strength. During the calibration process, these microproperties are systematically varied until the desired macro behavior is achieved. Table 2 shows the BPM microproperties used to replicate the average and lower estimate strength properties for each geologic unit. In all units, the interparticle and bond shear stiffnesses were equal to 57 percent of the normal stiffnesses, and the bond shear strength was equal to the bond normal strength. The interparticle friction coefficient is 0.6.

Table 2. BPM microproperties for the average and lower material estimates for the Richmond Hill (RH) and Redcliffs (RC) sites. R_{avg} is the average particle radius, $k_{n(particle)}$ is the normal stiffness of the particle contacts, $k_{n(bond)}$ is the normal stiffness of the bond, N_{bond} is the normal (tensile) strength of the bond, and $\rho_{particle}$ is the particle density.

	Layer	r_{avg} [m]	$k_{n(particle)}$ [N/m]	$k_{n(bond)}$ [N/m2]	N_{bond} [N/m2]	$\rho_{particle}$ [kg/m3]
Average	Columnar Basalt Lava (RH)	0.45	2.05E+07	8.26E+12	5.50E-01	3192
	Trachyte Lava Breccia (RH)	0.45	2.05E+07	8.26E+12	5.00E-02	2508
	Trachyte Lava Breccia (RH)	0.45	4.81E+07	1.94E+13	1.50E+00	2964
	Upper Breccia (RC)	0.45	5.82E+06	2.35E+12	1.70E-02	2052
	Columnar Basalt Lava (RC)	0.45	2.63E+07	1.06E+13	2.00E+00	3192
	Epiclastics (RC)	0.45	9.09E+06	3.67E+12	4.70E-02	2166
	Lower Breccia (RC)	0.45	4.45E+06	1.80E+12	2.70E-02	2166
Lower	Columnar Basalt Lava (RH)	0.45	2.05E+07	8.26E+12	2.00E-01	3192
	Trachyte Lava Breccia (RH)	0.45	2.05E+07	8.26E+12	3.00E-02	2508
	Trachyte Lava Breccia (RH)	0.45	4.81E+07	1.94E+13	1.01E+00	2964
	Upper Breccia (RC)	0.45	5.82E+06	2.35E+12	1.30E-02	2052
	Columnar Basalt Lava (RC)	0.45	2.63E+07	1.06E+13	1.50E+00	3192
	Epiclastics (RC)	0.45	9.09E+06	3.67E+12	3.70E-02	2166
	Lower Breccia (RC)	0.45	4.45E+06	1.80E+12	1.80E-02	2166

Boundary Conditions

The model boundary conditions are defined by viscous stress-controlled boundaries after the method developed by Lysmer and Kuhlemeyers (1969). The stresses are described by

$$\sigma = \rho V_p \omega' \quad (1)$$

and

$$\tau = \rho V_s u' \quad (2)$$

where σ and τ are the normal and shear stress, respectively; ρ is the material density; ω and u are the normal and tangential velocities, respectively; and V_p and V_s are the P-wave and S-wave velocities, respectively. The stress-controlled boundaries on the model absorb s-waves at the base of the model and s- and p-waves on the sides of the model, where free-field conditions are imposed using a viscous connection to 1-D response columns.

Ground Motions

The two site models were both subjected to the M_w 6.2 February 22nd, 2011 strong ground motion which was by far the most destructive event of the Canterbury Earthquake sequence. The horizontal components of the Lyttelton Port Company (LPCC) station recording were used as inputs. The LPCC station sits on a weak rock site (Site Class B) and is within 5.25 km of the two rock-slopes. According to the LPCC station recording, this earthquake had a peak horizontal acceleration of 0.92g (Bradley et al., 2014).

Results

Dynamic Stresses

The dynamic stresses induced in the uniform slope can be seen in Figure 2. The figure shows the magnitude of the change in the first invariant of the stress tensor due to the application of a shear pulse wavelet to the system. The first invariant of the stress tensor is directly related to the magnitude of volumetric stresses in the material. At t = 0.55s, the pulse is just encountering the toe of the slope and localized compression at the toe can be seen.

At t = 0.75s and t = 0.81s, local concentrations of volumetric expansion can be clearly observed near the slope face. Volumetric expansion can be extremely destructive in rock, even at moderate magnitudes due to the relatively low tensile strength of fractured rock masses and their stress-dependent shear strength. The color scale in the figures is set such that the ‘hot’ and ‘cold’ maximums correspond to a percentage of the nominal shear stress of the applied pulse. In this case, the magnitude of the volumetric expansive stresses at the slope face is approximately equal to 40 percent of the shear stress of the applied pulse.

Cliff Collapse

When subjected to the February 22, 2011 ground motion, the Richmond Hill and Redcliffs models experienced *cliff collapse* similar to that observed in the field. Tables 3 and 4 show the depth of *cliff collapse* for each geologic layer for the 4 unique models for Richmond Hill and Redcliffs. The tables also show the observed depths of collapse in the field. The relatively small variation in the depth of material loss between unique models indicates that the observed behavior is not being controlled by the particle packing structure. Figure 3 shows an example of the post-shaking configuration from models of each site. The models capture the trends of relative depth of material loss well and in some cases replicate the actual observed field behavior. For example, localized sections of overhanging geometry were observed at Richmond

Hill, and were also present in the model results. At Redcliffs, benching of the slope face at layer interfaces was observed and a similar pattern can be seen in some of the Redcliffs simulation results.

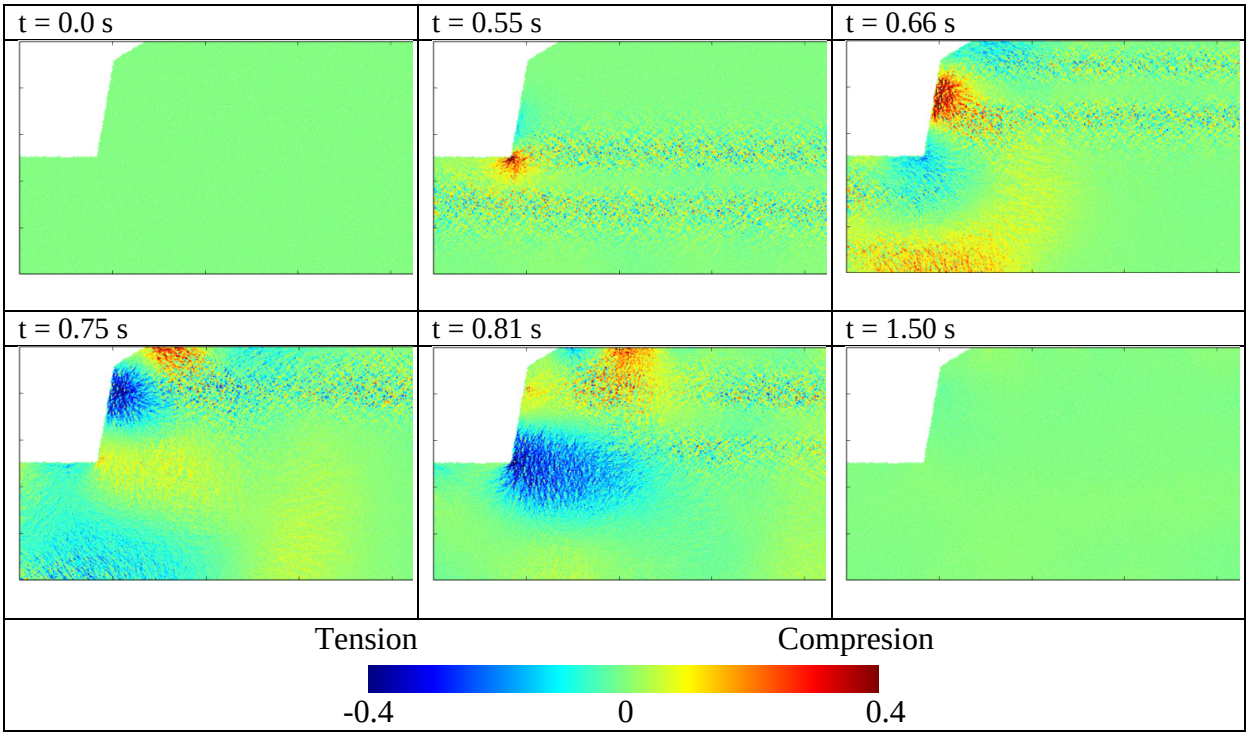

Figure 2. Change in first stress tensor invariant (volumetric stresses) in a rock-slope induced by an upward propagating shear pulse. The extremes of the colormap correspond to a stress magnitude equal to 40 percent of the input shear wave stress magnitude. Blue indicates tension. Red indicates compression.

Table 3. Depth of material loss for the Richmond Hill site in meters.

Layer	Richmond Hill 1	Richmond Hill 2	Richmond Hill 3	Richmond Hill 4	Richmond Hill Average	Field
1-Basalt Lava Breccia	0	0	0.5	0	0.13	up to 2
2-Trachyte Lava Breccia	0.5	2	1	1	1.13	up to 2
3-Trachyte Lava	0	0	0	0	0	covered by talus

Table 4. Depth of material loss for the Redcliffs site in meters.

Layer	Redcliffs 1	Redcliffs 2	Redcliffs 3	Redcliffs 4	Redcliffs Average	Field
1-Upper Breccia	10	10	12	8	10.0	up to 6
2-Basalt Lava	8	4	8	6	6.5	up to 6
3-Epiclastics	6	4	6	6	5.5	up to 6
4-Lower Breccia	6	4	6	4	5.0	covered by talus

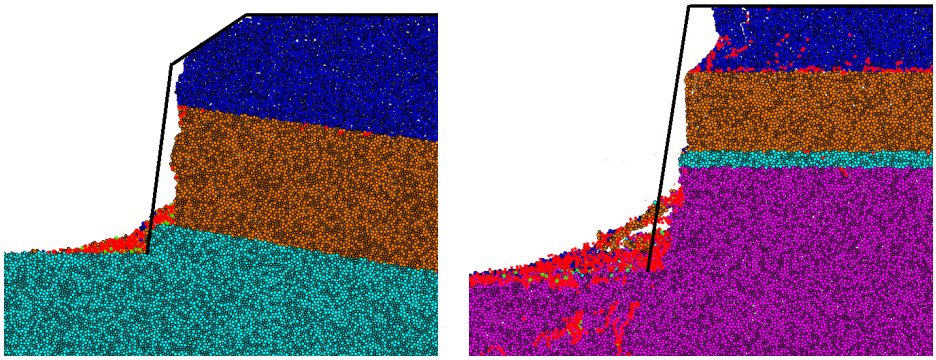

Figure 3. Post-earthquake configurations of the PFC models of the Richmond Hill (left) and Redcliffs (right) sites. The original slope geometry, outlined in black, shows the relatively shallow nature of the *cliff collapse* mechanism. New fractures are shown in red.

In order to isolate the effects of the reduced strength weathering zone and the pre-existing fractures, separate simulations that included the weathering effect, but no fractures, were run. Without the inclusion of fractures in the models only one of the eight models tested experienced any damage due to the strong ground motion. This demonstrates that the reduced strength due to weathering alone is not driving the result.

Cliff Top Displacement

The PFC models do not adequately predict the *cliff top displacement* that were observed in the field at both sites. Figure 4 shows the average PFC *cliff top displacement* for the Richmond Hill models along with the measured field displacements. A comparison of results for the Redcliffs site (not shown) also shows that the PFC model significantly under-predicts the *cliff top displacement*. This discrepancy is most likely due to the inherent limitations of BPM. Because the particles themselves are rigid, deformations are limited to the inter-particle contacts. The ability BPM to accumulate deformation in damaged material is, therefore, a function of resolution of the model.

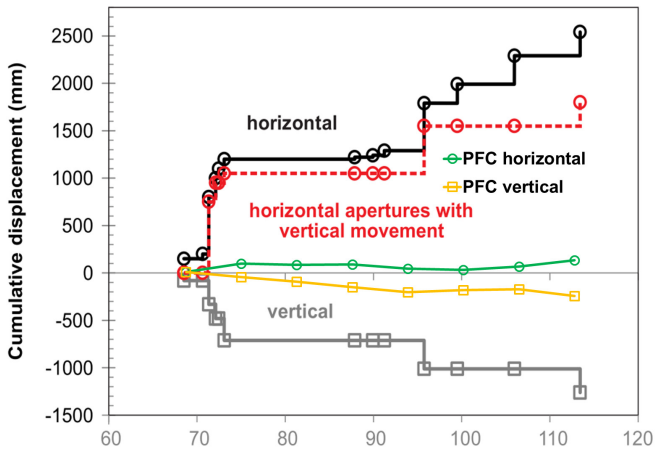

Figure 4. *Cliff top displacement* at Richmond Hill from field measurements (shown in black, red, and gray) and PFC model results (green and yellow). The PFC models significantly underestimate the *cliff top displacement* profile.

Conclusions

The seismically-induced *cliff collapse* observed throughout the Port Hills area during the Canterbury Earthquake Sequence cannot be adequately evaluated with traditional rock-slope analysis methods. Using a fully dynamic bonded particle model, the *cliff collapse* at two Port Hills sites was successfully modeled. The model results indicate that these collapses were due to a combination of weathering, fractures, and dynamic stress conversions near the slope face. The PFC model was unable to capture the *cliff top displacement* at the level of resolution used. This indicates that although BPM is a powerful tool, it may only be appropriate for use as a supplement to, rather than a replacement for, traditional methods.

Acknowledgements

Financial support for this research was provided by the United States National Science Foundation (NSF) under grant CMMI-1156413.

References

Bradley, Brendon a., Mark C. Quigley, Russ J. Van Dissen, and Nicola J. Litchfield. 2014. “Ground Motion and Seismic Source Aspects of the Canterbury Earthquake Sequence.” *Earthquake Spectra*.

Lysmer, John, and Roger L. Kuhlemeyer. 1969. “Finite Dynamic Model for Infinite Media.” *Journal of the Engineering Mechanics Division*.

Mas Ivars, Diego, Matthew E. Pierce, Caroline Darcel, Juan Reyes-Montes, David O. Potyondy, R. Paul Young, and Peter a. Cundall. 2011. “The Synthetic Rock Mass Approach for Jointed Rock Mass Modelling.” *International Journal of Rock Mechanics and Mining Sciences*.

Massey, C. I., M McSaveney, D Heron, and B Lukovic. 2012. *Canterbury Earthquakes 2010/11 Port-Hills Slope Stability: Pilot Study for Assessing Life-Safety Risk from Rockfalls (boulder Rolls). GNS Science Consultancy Report*.

Massey, Chris I., Mauri J. McSaveney, Tony Taig, Laurie Richards, Nicola J. Litchfield, David a. Rhoades, Graeme H. McVerry, et al. 2014(a). “Determining Rockfall Risk in Christchurch Using Rockfalls Triggered by the 2010-2011 Canterbury Earthquake Sequence.” *Earthquake Spectra*.

Massey, C. I., T. Taig, B Lukovic, W Ries, F Della Pasqua, and G Archibald. 2014(b). *Canterbury Earthquakes 2010 / 11 Port Hills Slope Stability : Debris Avalanche Risk Assessment for Richmond Hill*.

Massey, C. I., T. Taig, B Lukovic, W Ries, F Della Pasqua, G Archibald, and D Heron. 2014(c). *Canterbury Earthquakes 2010 / 11 Port Hills Slope Stability : Risk Assessment for Redcliffs*.

Potyondy, D.O., and P.a. Cundall. 2004. “A Bonded-Particle Model for Rock.” *International Journal of Rock Mechanics and Mining Sciences*.